Asian Journal of Chemistry; Vol. 35, No. 9 (2023), 2148-2152

ASIAN JOURNAL OF CHEMISTRY

https://doi.org/10.14233/ajchem.2023.28056

$La_{10}Si_6O_{27}:Eu^{3+}$ Nanophosphor: Its Photocatalytic and Sensor Applications

A. Naveen Kumar[1], N. Basavaraju[2], C.R. Ravikumar[2,*], V.G. Dileepkumar[3,4], R. Ramesh[5] and H.C. Ananda Murthy[6,*]

[1]Department of Physics, South East Asian College of Engineering and Technology (Affiliated to Visvesvaraya Technological University), Bangalore-560049, India
[2]Department of Science, East West Institute of Technology (Affiliated to Visvesvaraya Technological University), Bangalore-560091, India
[3]Department of Chemistry, HKBK College of Engineering Bangalore-560045, India
[4]Department of Chemistry, PES University, BSK 3rd Stage, Bangalore-560085, India
[5]Department of Chemical Engineering, School of Mechanical, Chemical and Materials Engineering, Adama Science and Technology University, P.O. Box 1888, Adama, Ethiopia
[6]Department of Physical and Chemical Sciences, School of Science, Sri Sathya Sai University for Human Excellence, Sri Sathya Sai Grama, Chikkaballapur-562101, Karnataka, India

*Corresponding author: E-mail: ravicr128@gmail.com

Received: 30 May 2023; *Accepted*: 12 July 2023; *Published online*: 31 August 2023; AJC-21356

This study reported the influence of $La_{10}Si_6O_{27}:Eu^{3+}$ nanophosphor prepared by solution combustion method by using oxalyl dihydrazide as fuel on the electrochemical performance in HCl used as an electrolyte. The structural morphology of the nanoparticles was characterized by PXRD, it confirms pure hexagonal oxyapatite phase with the crystallite size averaging between 20-30 nm. To examine the electrochemical behaviour of the nanophosphor in an acidic medium, both electrochemical impedance spectroscopy (EIS) and cyclic voltammetry (CV) techniques were utilized. For the electrochemical analysis used in this study, a modified carbon paste electrode (CPE) with the nanophosphor was utilized as the working electrode, which is an excellent sense of the paracetamol and sildenafil citrate (viagra). Further, the synthesized $La_{10}Si_6O_{27}:Eu^{3+}$ nanophosphor exhibited improved photocatalytic mobility (PCM) and enhanced photostability when exposed to UV light during the decomposition process of direct green dye. These findings suggest that the developed material holds great promise as a potential sensor and photocatalyst.

Keywords: Nanophosphor, Photocatalytic activity, Carbon paste electrode, Direct green dye, Sensor.

INTRODUCTION

In recent years, several researchers have been interested inorganic nanomaterials especially rare earth based nanomaterials due to their unique chemical properties and physical properties as they possess better catalytic activity in nanoscale than in bulk materials [1,2]. Research on inorganic nanostructured materials encompasses the investigation and development of materials with nanoscale dimensions, primarily composed of inorganic elements. These materials exhibit unique properties and behaviours at the nanoscale, making them highly attractive for a wide range of applications in fields such as electronics, catalysis, energy and medicine. The work done in this area focuses on understanding the synthesis, characterization and manipulation of inorganic nanostructured materials. Various techniques, including chemical synthesis, physical vapour deposition and template assisted methods, are employed to fabricate nanostructures with precise control over their size, shape, composition and surface properties. The properties of inorganic nanostructured materials are influenced by quantum confinement, surface effects and the high surface-to-volume ratio, leading to enhanced mechanical, electrical, optical and catalytic properties [3,4]. Researchers aim to explore and exploit these unique characteristics to develop advanced materials with improved performance and novel functionalities. The exploration of novel fabrication techniques, such as bottom-up self-assembly and top-down lithography, is crucial for achieving precise control over nanoscale structures and integrating them into practical devices and systems [5-7].

The lighting industry is currently focusing on solid-state lighting, which utilizes light-emitting diodes (LEDs) and luminescent phosphor materials to produce white light. The design of bright and stable phosphors plays a crucial role in this field. White light-emitting diodes (WLEDs) have the capability to save approximately 70% of energy and eliminate the need for harmful ingredients found in traditional light sources such as incandescent light bulbs and fluorescent tubes [8-11]. As a result, WLEDs possess enormous potential to replace these conventional options and these solid-state lighting devices are widely regarded as the next evolutionary leap in lighting technology. Lanthanides possess the distinctive feature of having an incompletely filled 4*f*-shell, exhibit the ability to absorb excitation energy in the excited state and subsequently emit light in the visible region upon returning to the ground state. Lanthanides exhibit numerous efficient and tightly focused emission lines within the visible region. These emission lines remain relatively unaffected by their surrounding matrices, thanks to the shielding effect provided by the outer 5*s* and 5*p* electrons [12].

The present study involved in the effectively synthesized samples of $La_{10}Si_6O_{27}$ doped with Eu^{3+} using the solution combustion method. The synthesized samples were characterized utilizing sophisticated instruments. The present study aimed to explore the photocatalytic and electrochemical properties of $La_{10}Si_6O_{27}$ samples doped with Eu^{3+}.

EXPERIMENTAL

Synthesis: For the preparation of $La_{10}Si_6O_{27}:Eu^{3+}$ (1-9 mol %), a suitable amount of lanthanum nitrate ($La(NO_3)_3.6H_2O$ (Sigma Aldrich) and fumed silica SiO_2 (Sigma Aldrich) was purchased and mixed in stoichiometric ratios with the prepared oxalyl dihydrazide (ODH; $C_2H_6N_4O_2$) fuel to introduce dopant material, $Eu(NO_3)_2$ was added to a minimal amount of double-distilled water in a petri dish and thoroughly mixed using a magnetic stirrer for approximately 15 min. The combustion synthesis involved a specific stoichiometry of the redox mixture, which was determined by considering the total oxidizing and reducing valences of the compounds [1]. The petri dish containing the heterogeneous mixture was then placed into a muffle furnace, maintained at a temperature of 450 ± 10 ºC. Initially, the solution underwent boiling and dehydration, leading to the decomposition of the mixture and the release of significant amounts of gases, including N_2, H_2O and CO_2. Upon the surface of foam, a flame ignited and swiftly spread throughout the entire volume, leading to the formation of a white powder. Subsequently, a foam-like product remained in the petri dish, which was then finely powdered using a laboratory agate. The powders were then subjected to calcination at 950 ºC for 3 h. By considering a complete combustion of the precursors, the balanced chemical equation can be written as follows:

$$10La[NO_3]_3{\cdot}6H_2O + 6SiO_2 + 15C_2H_6N_4O_2[ODH] \longrightarrow La_{10}Si_6O_{27} + 105H_2O + 30CO_2 + 45N_2 \quad (1)$$

Characterization: The powder samples were subjected to PXRD analysis to determine their crystalline nature. This analysis was conducted using an X-ray diffractometer from Shimadzu. The instrument operated at 50 kV and 20 mA, utilizing Cu*K*α radiation with a wavelength of 1.541 Å. A nickel filter was employed and the scan rate was set at 20 min^{-1}. For transmission electron microscopy (TEM) analysis, a JEOL JEM-2100 instrument equipped with an EDS system was utilized. The accelerating voltage was capable of reaching up to 200 kV and a LaB6 filament was employed. The TEM had a resolution of 1.5 Å. UV-visible studies of the samples were performed using Shimadzu's uv-26000 instrument. The measurements were conducted within the range of 200 to 800 nm. To investigate the photoluminescence properties, Horiba's Fluorolog-3 spectrofluorometer was employed. The experiments were carried out at room temperature using a 450 W xenon lamp as the excitation source. Spectral analysis was performed using the Fluor Essence™ software. PXRD analysis was also utilized to study the crystalline nature and phase of the final product. The cyclic voltammetry (CV) tests were conducted using a CHI608E potentiostat. A three-electrode system consisting of a nanomaterial coated with carbon paste electrode, a platinum wire and an Ag/AgCl electrode was employed as the working, counter and reference electrodes, respectively. The tests were performed in 6 M HCl and different scan rates of 10, 20, 30, 40 and 50 mV/s were used. The potential variation ranged from -0.8 to 1 V relative to the Ag/AgCl electrode.

RESULTS AND DISCUSSION

PXRD studies: The PXRD patterns displayed in Fig. 1 illustrate the characteristics of $La_{10}Si_6O_{27}$ nanophosphors doped with Eu^{3+} at concentrations ranging from 1 to 9 mol%. The samples were synthesized using a combustion synthesis method, resulting in a pure hexagonal oxyapatite phase. The observed X-ray diffraction peaks in the samples were accurately matched and then indexed with JCPDS card No. 00-053-0291 [11]. By utilizing Scherrer's equation, the average particle size (D) of the nanophosphors was estimated to be within the range of 20-25 nm [2]:

$$D = \frac{K\lambda}{\beta\cos\theta} \quad (2)$$

where 'K' represents a constant, 'λ' represents the wavelength of X-rays and 'β' represents the full width at half maximum (FWHM) value.

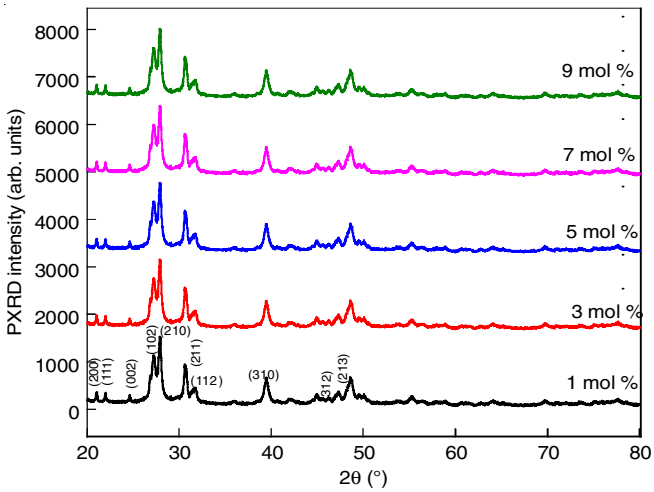

Fig. 1. PXRD patterns of $La_{10}Si_6O_{27}:Eu^{3+}$ (1-9 mol%) nanophosphors

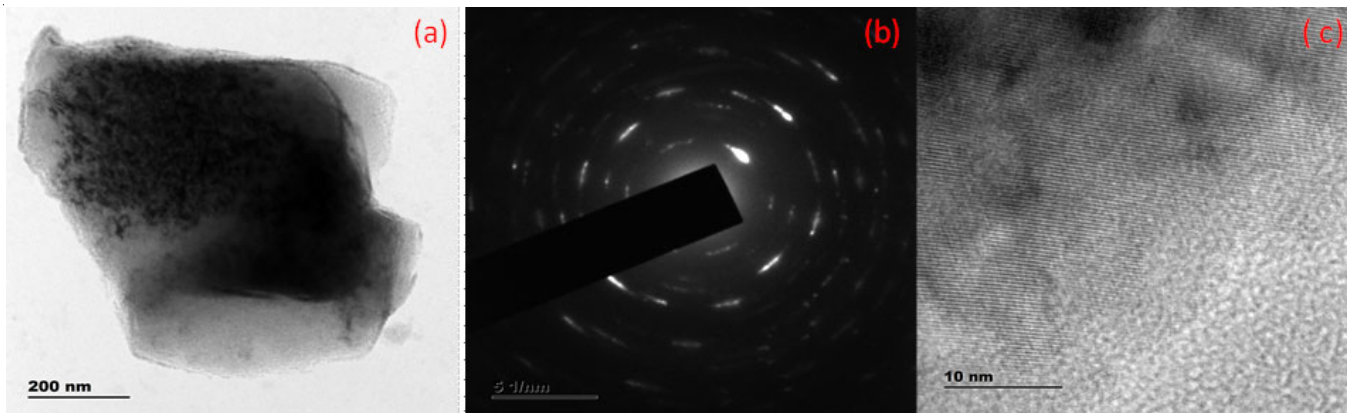

Fig. 2. (a) TEM image (b) SAED and (c) HRTEM of $La_{10}Si_6O_{27}:Eu^{3+}$

TEM studies: TEM image reveals the presence of nearly spherical-shaped particles (Fig. 2a) within a size range of 20-25 nm. The polycrystalline nature was confirmed by the selected area electron diffraction (SAED) pattern. The samples demonstrate a notable level of crystallinity, which is evident from the presence of clearly defined lattice fringe patterns [13]. Notably, the grain boundary formed by silica is continuous and devoid of any gaps. According to the SEAD analysis, this silica is amorphous, which aligns with the observations (Fig. 2b). The core of the particles exhibits the same crystallographic planes. High-resolution TEM imaging and SAED patterns further indicate the presence of an amorphous silica phase and an orthorhombic $La_{10}Si_6O_{27}$ crystallographic phase, which corroborates well with the XRD analysis [14].

Photodegradation of direct green dye: Fig. 3 presents the photocatalytic activities of synthesized $La_{10}Si_6O_{27}$ assessed through the degradation of direct green under UV light irradiation. It is demonstrated that $La_{10}Si_6O_{27}:Eu^{3+}$ exhibited notable photocatalytic activity within 120 min due to the efficient and rapid combination of electrons and holes. After 60 min, the sample achieved a 50% decolourization of direct green dye, whereas $La_{10}Si_6O_{27}$ nanoparticles displayed lower effectiveness in direct green decolourization. Over time, a gradual decrease in direct green dye concentrations was observed in the presence

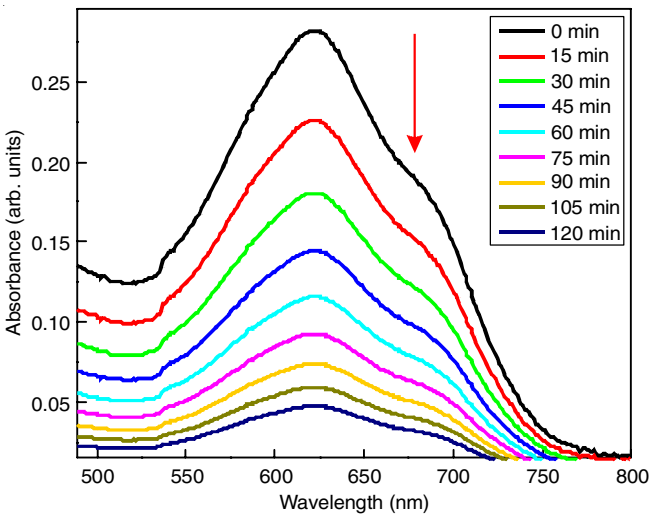

Fig. 3. Absorbance spectra of $La_{10}Si_6O_{27}:Eu^{3+}$ under UV radiation

of $La_{10}Si_6O_{27}$ nanoparticles, reaching approximately 80% decolourization after 120 min of UV illumination. Moreover, the UV-visible analysis revealed the absence of any intermediate product, suggesting that over 80% of direct green dye degraded within the 120 min of UV light exposure period. Furthermore, to understand the decolonization efficiency using eqn. 3:

$$\frac{\log c}{C_o} = -k_t \quad (3)$$

The relationship between log C/C_o and k, where C_o represents the dye concentration at t = 0 min, C represents the dye concentration at the testing time and k is the rate constant for a first-order reaction. The calculated values exhibited a linear correlation, confirms first-order kinetics. The slope k, was determined to be 0.020 min^{-1} and 0.010 min^{-1} for direct green dye, respectively. Additionally, the photocatalytic decolourization efficiency of the direct green dye was calculated using eqn. 4:

$$D\ (\%) = \frac{C_o - C}{C_o} \times 100 \quad (4)$$

The photo-decolourization efficiency (%D) was calculated based on the process of photocatalytic degradation of direct green dye by $La_{10}Si_6O_{27}$ and can be elucidated by considering the the concentration of dye used before and after the degradation (at certain time t). This mechanism provides insights into the overall photo-decolourization process.

Electrochemical sensor: The carbon paste electrode, prepared freshly, served as the working electrode in this study. To evaluate its electrochemical properties and performance as a Faradaic supercapacitor, a standard three-electrode experimental cell configuration was utilized. The cell was equipped with a counter electrode made of platinum wire, a working electrode and a reference electrode consisting of Ag/AgCl. The electrochemical measurements used in this study were conducted using a 1 M HCl solution as the acidic electrolyte. The measurements, including AC impedance and cyclic voltammetry (CV) were performed at room temperature.

In Fig. 4, the CV curves of 3 mol% Eu^{3+}-doped $La_{10}Si_6O_{27}$ sample in a 1 M HCl electrolyte are displayed at a scan rate of 10 mV s^{-1}. The obtained curve for all scan rates demonstrates the presence of a pseudo-capacitance, indicating the occurrence of both oxidation and reduction reactions [15].

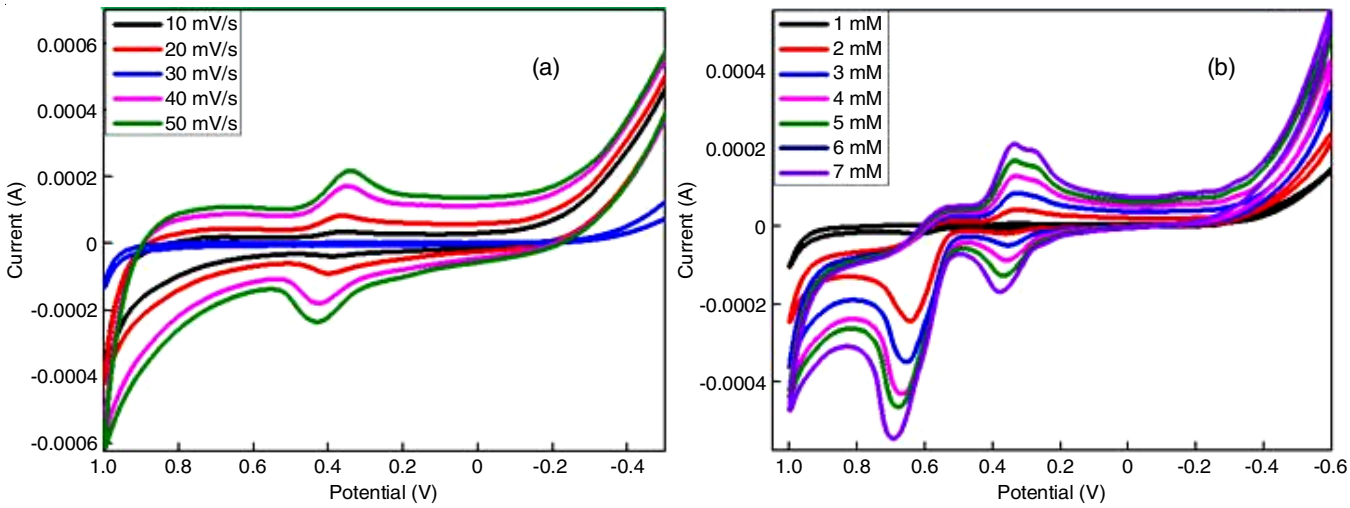

Fig. 4. (a) Cyclic voltammogram of $La_{10}Si_6O_{27}$ electrode, (b) sensor detection of penagra in the concentration range 1-6 mM

The specific capacitance of an electrode is typically associated with the area under its cyclic voltammetry curve. The reversibility of redox reactions can be evaluated by analyzing the cyclic voltammetry curves, particularly by examining the difference in peak potentials (E_O-E_R) between the anodic (E_O) and cathodic (E_R) peaks. A smaller E_O-E_R value indicates a more reversible electrode reaction [9]. In case of $La_{10}Si_6O_{27}$ doped Eu^{3+} electrodes, a comparison was made and the cyclic voltammogram revealed an anodic oxidation peak potential of 0.430 V and a cathodic reduction peak potential of 0.343 V.

Fig. 4a-b illustrate the cyclic voltammograms obtained from the utilization of $La_{10}Si_6O_{27}$ for the detection of sildenafil citrate. A significant shift in the positions of the oxidation and reduction peaks is observed, confirming the effectiveness of carbon paste electrodes prepared with $La_{10}Si_6O_{27}$ as a material for electrochemical applications in an acidic medium (HCl) for sildenafil citrate solutions ranging from 1 mM to 6 mM. The $La_{10}Si_6O_{27}$ electrode exhibits an anodic oxidation peak at -0.695 V and a cathodic reduction peak at -0.337 V (Fig. 4b).

From the cyclic voltammetry (CV) studies, a notable observation is made due to the emergence of an additional reduction peak around -0.337 V. As a consequence, the previously observed cathodic reduction peak at -0.695 V completely disappears. Furthermore, the oxygen evolution peak is no longer visible in the CV data. The $La_{10}Si_6O_{27}$ carbon paste electrode demonstrates an initial current response to 1 mM sildenafil citrate. Furthermore, with successive injections of 6 mM sildenafil citrate solution at an interval of 50 s, the current response gradually increases and reaches a steady-state current within a short period of 3 s. This behaviour signifies that the proposed sensor demonstrates a swift response to the oxidation of sildenafil citrate. It is interesting to note that the sensitivity of the sensor material developed for the purpose of detecting sildenafil citrate solutions has been improved.

Conclusion

The red-emitting $La_{10}Si_6O_{27}:Eu^{3+}$ (1-9 mol%) nanophosphors were prepared using oxalyl dihydrazide (ODH) as fuel using a low-temperature solution combustion method. The PXRD patterns confirmed that the nanophosphors were in a pure hexagonal oxyapatite phase, with an average crystallite size ranging from 20 to 25 nm. Both the analytical techniques HRTEM and PXRD analysis confirms the presence of a pure monoclinic phase in the $La_{10}Si_6O_{27}$ nanoparticles, while electron microscopic analysis uncovered the agglomerated, spongy and porous nature of synthesized $La_{10}Si_6O_{27}$ sample. The prepared electrode using $La_{10}Si_6O_{27}$ nanoparticles demonstrated a good reversibility, as indicated by a lower value of peak potential difference (E_O-E_R) in cyclic voltammetry (CV) measurements. These electrodes exhibited high effectiveness in sensing sildenafil citrate in an acidic medium (HCl). Another crucial finding of the present study is the ease of synthesis of the material and the straightforward fabrication of the working electrode. Furthermore, the material exhibits enhanced stability towards both oxidation and reduction reactions. Additionally, it is noteworthy that the material demonstrates high sensitivity towards the selected drug molecule. Furthermore, the photocatalytic properties of $La_{10}Si_6O_{27}$ were also evaluated, exhibiting that more than 80% of direct green dye experienced photo- decolourization when exposed to UV light for 120 min. These results highlight the promising and cost-effective nature of $La_{10}Si_6O_{27}$ as an electrode material for future sensor and photocatalytic applications.

ACKNOWLEDGEMENTS

The authors thank Vision Group on Science and Technology (VGST), Govt. of Karnataka, India, (No: VGST/CISEE/2014-15/282) and (VGST/K-FIST-L1/2014-15/GRD-360) for extending their support to carry out this research work.

CONFLICT OF INTEREST

The authors declare that there is no conflict of interests regarding the publication of this article.

REFERENCES

1. H. Zhao, J. Xia, D. Yin, M. Luo, C. Yan and Y. Du, *Coord. Chem. Rev.*, **390**, 32 (2019); https://doi.org/10.1016/j.ccr.2019.03.011

2. S. Ashwini, S.C. Prashantha, R. Naik and H. Nagabhushana, *J. Rare Earths*, **37**, 356 (2019); https://doi.org/10.1016/j.jre.2018.07.009
3. K.M. Girish, S.C. Prashantha, H. Nagabhushana, H.P. Nagaswarupa, R. Naik, K.S. Anantha Raju, H.B. Premkumar, S.C. Sharma and B.M. Nagabhushana, *Spectrochim. Acta A Mol. Biomol. Spectrosc.*, **138**, 857 (2015); https://doi.org/10.1016/j.saa.2014.10.097
4. T. Manohar, R. Naik, S.C. Prashantha, H. Nagabhushana, S.C. Sharma, H.P. Nagaswarupa, K.S. Anantharaju, C. Pratapkumar and H.B. Premkumar, *Dyes Pigments*, **122**, 22 (2015); https://doi.org/10.1016/j.dyepig.2015.06.002
5. S. Bhattacharya, A.K. Agarwal, N. Chanda, A. Pandey and A. Kumar Sen, Environmental, Chemical and Medical Sensors, Springer Nature, Singapore: Springer, pp. 167-198 (2018).
6. K. Wang, Q. Ma, C.-X. Qu, H.-T. Zhou, M. Cao and S.-D. Wang, *Autex Res. J.* (2022); https://doi.org/10.2478/aut-2022-0014
7. Z. Chai, A. Childress and A.A. Busnaina, *ACS Nano*, **16**, 17641 (2022); https://doi.org/10.1021/acsnano.2c07910
8. A. Brisse, A.L. Sauvet, C. Barthet, S. Georges and J. Fouletier, *Solid State Ion.*, **178**, 1337 (2007); https://doi.org/10.1016/j.ssi.2007.07.009
9. T. Liao, T. Sasaki, S. Suehara and Z. Sun, *J. Mater. Chem.*, **21**, 3234 (2011); https://doi.org/10.1039/c0jm02473b
10. E.V. Tsipis, V.V. Kharton and J.R. Frade, *Electrochim. Acta*, **52**, 4428 (2007); https://doi.org/10.1016/j.electacta.2006.12.025
11. D. Li, M. Li, Y. Zhang, G. Zhu and X. Wang, *Int. J. Electrochem. Sci.*, **11**, 9783 (2016); https://doi.org/10.20964/2016.12.12
12. M.M. Mezdrogina and E.Yu. Danilovskii and R.V. Kuz'min, *Inorg. Mater.*, **47**, 1450–1469 (2011); https://doi.org/10.1134/S0020168511130048
13. H. Liu, Y. Hao, H. Wang, J. Zhao, P. Huang and B. Xu, *J. Lumin.*, **131**, 2422 (2011); https://doi.org/10.1016/j.jlumin.2011.05.042
14. G. Ramakrishna, H. Nagabhushana, B.D. Prasad, Y.S. Vidya, S.C. Sharma, K.S. Anantharaju, S.C. Prashantha and N. Choudhary, *J. Lumin.*, **181**, 153 (2017); https://doi.org/10.1016/j.jlumin.2016.08.050
15. B. Avinash, C.R. Ravikumar, M.R.A. Kumar, H.P. Nagaswarupa, M.S. Santosh, A.S. Bhatt and D. Kuznetsov, *J. Phys. Chem. Solids*, **134**, 193 (2019); https://doi.org/10.1016/j.jpcs.2019.06.012